View metadata, citation and similar papers at core.ac.uk
brought to you by CORE
provided by AIR Universita degli studi di Milano

Nuclear-matter distribution in the proton-rich nuclei ^{7}Be and ^{8}B from intermediate energy proton elastic scattering in inverse kinematics

A.V. Dobrovolsky[a,*], G.A. Korolev[a], A.G. Inglessi[a], G.D. Alkhazov[a], G. Colò[b], I. Dillmann[c], P. Egelhof[c], A. Estradé[c], F. Farinon[c], H. Geissel[c], S. Ilieva[c], Y. Ke[c], A.V. Khanzadeev[a], O.A. Kiselev[c], J. Kurcewicz[c], X.C. Le[c], Yu.A. Litvinov[c], G.E. Petrov[a], A. Prochazka[c], C. Scheidenberger[c], L.O. Sergeev[a], H. Simon[c], M. Takechi[c], S. Tang[c], V. Volkov[c], A.A. Vorobyov[a], H. Weick[c], V.I. Yatsoura[a]

[a] *Petersburg Nuclear Physics Institute, National Research Centre Kurchatov Institute, Gatchina, 188300 Russia*
[b] *Dipartimento di Fisica, Università degli Studi di Milano, 20133 Milano, Italy*
[c] *GSI Helmholtzzentrum für Schwerionenforschung GmbH 64291 Darmstadt, Germany*

Abstract

Absolute differential cross sections for elastic p^{7}Be and p^{8}B small-angle scattering were measured in inverse kinematics at an energy of 0.7 GeV/u at GSI Darmstadt. The hydrogen-filled ionization chamber IKAR was used as an active target to detect the recoil protons. The projectile tracking and isotope identification were performed with multi-wire proportional chambers and scintillation detectors. The measured cross sections were analysed using the Glauber multiple-scattering theory. The root-mean-square (rms) nuclear matter radii $R_{\rm m} = 2.42(4)$ fm for ^{7}Be and $R_{\rm m} = 2.58(6)$ fm for ^{8}B were obtained. The radial density distribution deduced for ^{8}B exhibits a halo structure with the rms halo radius $R_{\rm h} = 4.24(25)$ fm. The rms proton radius of the proton-rich ^{8}B is found to be $R_{\rm p} = 2.76(9)$ fm and is significantly larger than those of the stable isotopes ^{10}B and ^{11}B. A comparison of the deduced experimental radii is made with existing experimental and theoretical data.

Keywords: ^{8}B, ^{7}Be, nuclear matter distribution, nuclear matter radii, proton-nucleus elastic scattering

1. Introduction

The recent development of radioactive isotope beam techniques has opened excellent opportunities to study the structure of light unstable nuclei far from the valley of stability. Among others, new properties of the nuclear matter were discovered. The weak binding of the last bound nucleons causes the formation of neutron (proton) skins on the surface of the nucleus and the formation of a halo structure [1–4]. It has been found that the existence of a halo corresponds to a large extension of the matter density distribution beyond the nuclear core. The halo structure manifests itself by large interaction (reaction) cross sections, by increased removal nucleon cross sections and by narrow momentum distributions of reaction products in the processes of nuclear break-up and Coulomb dissociation. An increase in the root-mean-square (rms) radius $R_{\rm m}$ of the radial distribution of the nuclear matter in nuclei near the neutron drip line was the first indication of a halo in exotic nuclei such as ^{6}He, ^{11}Li, ^{11}Be and ^{14}Be [3, 4]. These investigations showed that most of the halo nuclei have neutron halos, while the formation of proton halos is much less probable due to the Coulomb barriere effect [1].

The proton drip-line nucleus ^{8}B is considered to be the most interesting candidate for the occurrence of a proton halo since it has a very small proton separation energy $S_{\rm p} = 136.4$ keV [5]. The study of the proton-rich nuclei ^{8}B and ^{7}Be (^{7}Be being the presumable core in ^{8}B) are important for both nuclear

*Corresponding author
Email address: Dobrovolsky_AV@pnpi.nrcki.ru (A.V. Dobrovolsky)

physics and astrophysics. These nuclei play an essential role in the solar neutrino problem. The ^{8}B nucleus is produced in the Sun through the ^{7}Be$(p,\gamma)^8$B reaction at the centre of mass energy $E_{\rm c.m.}$ of about 20 keV and emits a high energy neutrino, which can be detected in terrestrial experiments [6, 7]. The proton capture rate in ^{7}Be strongly depends on the ^{8}B structure. The size of ^{8}B and the shape of the proton density distribution at large distances determines the proton capture rate and are important to the solar neutrino issue [6–9]. It is a standard procedure to determine the magnitude of the $\sigma_{\rm p\gamma}(E_{\rm c.m.})$ cross section in terms of the astrophysical factor $S_{17}(E_{\rm c.m.}) = \sigma_{\rm p\gamma}(E_{\rm c.m.})E_{\rm c.m.}\exp(2\pi\eta)$, where η is the Sommerfeld parameter. Therefore, a better knowledge of S_{17} is important to improve the precision of theoretical predictions for the ^{8}B neutrino flux.

The ^{8}B proton-halo problem has received much attention from both experimental and theoretical points of view. The halo structure of ^{8}B was suggested for the first time by the Osaka group [10] to explain the unusually large quadrupole moment Q of this nucleus as compared to the value for the mirror nucleus ^{8}Li. The experimental data for Q were well reproduced by the wave function with a long proton tail obtained for ^{8}B in the shell model using the Cohen-Kurath interaction. Howerer, theoretical investigations [11, 12] have shown that the large quadrupole moment of ^{8}B can be explained without the existence of a proton halo. At present, the main evidence for the halo structure of ^{8}B is obtained from experiments on break-up reactions. The measurements of the momentum distribution of ^{7}Be fragments from the ^{8}B break-up reactions showed a much narrower distribution than the one for stable nuclei [13–17]. Moreover, the one-proton removal cross section is enhanced as compared to the case of a nucleus with a tightly bound proton [16–20], what is also a signature for an extended valence-proton wave function.

The size and the shape of the radial distribution of the nuclear matter are fundamental properties of nuclei and can be the most convincing evidence for the proton halo structure. The matter density distribution in ^{8}B was determined and the rms matter radius $R_{\rm m}$ was obtained in measurements of interaction or reaction cross sections [15, 19, 21–25]. However, the values of $R_{\rm m}$ deduced using different versions of the Glauber model are widely scattered, ranging from 2.38(2) fm to 2.61(8) fm. To reproduce reaction cross sections for ^{8}B measured at low energies, Warner *et al.* [22] used microscopic calculations with a matter distribution obtained by the Osaka group [10]. The nuclear properties of ^{8}B was the subject of much theoretical work performed in the last years, see Refs. [11, 26–37] and references therein.

Information on the structure of ^{7}Be, the presumable core of ^{8}B, is rather scarce. The matter radii $R_{\rm m} = 2.31(2)$ fm [21] and $R_{\rm m} = 2.36(6)$ fm [38] were obtained through measurements of the interaction and reaction cross sections. The proton radius $R_{\rm p}$= 2.507(17) fm [39] was derived from the charge radius $R_{\rm ch}$ measurement in a laser spectroscopy study [40]. The proton-rich ^{7}Be nucleus is a weakly bound two-body system with a separation energy of 1.59 MeV for break-up into ^{3}He and ^{4}He. The structure of ^{7}Be was discussed in many theoretical investigations [11, 15, 31–37, 41–43]. A cluster structure of ^{7}Be (as well as of the ^{8}B nucleus) was supposed in Refs. [11, 31, 33]. The large cross section (σ = 242 mb) for the He break-up channel measured at GANIL [15] supported the concept of the cluster structure for ^{7}Be.

The objective of the present work was to obtain in a single experiment information on the structure of ^{8}B and its supposed core nucleus ^{7}Be in order to derive a convincing conclusion about the existence of the halo in ^{8}B. The proton-nucleus elastic scattering at intermediate energies around 700–1000 MeV is considered as one of the best methods to determine matter density distributions in stable nuclei [1, 44, 45]. In order to study exotic nuclei, experiments in inverse kinematics using radioactive nuclear beams and the active target IKAR, a hydrogen-filled time projection ionization chamber, were proposed and then performed in a first experiment [46, 47]. It turned out that small angle proton scattering is particularly sensitive to the halo structure [46]. Therefore, in order to study the spatial structure of halo nuclei it is important to measure with high accuracy the absolute differential cross sections for proton elastic scattering at small momentum transfers. An analysis of the shape of the measured cross sections makes it possible to determine the nuclear matter distributions and radii of the nuclear cores and halos [46, 48]. In further experiments performed at GSI Darmstadt by the PNPI–GSI Collaboration the method has been successfully applied to study the stable ^{4}He, ^{6}Li and the neutron-rich isotopes ^{6}He, ^{8}He, ^{8}Li, ^{9}Li, ^{11}Li, ^{12}Be and ^{14}Be [48–52].

The present paper reports on new results obtained for proton-rich isotopes ^{7}Be and ^{8}B. The first results on the study of the ^{8}B structure in comparison with its mirror nucleus ^{8}Li were briefly presented in a Letter published in Ref. [53].

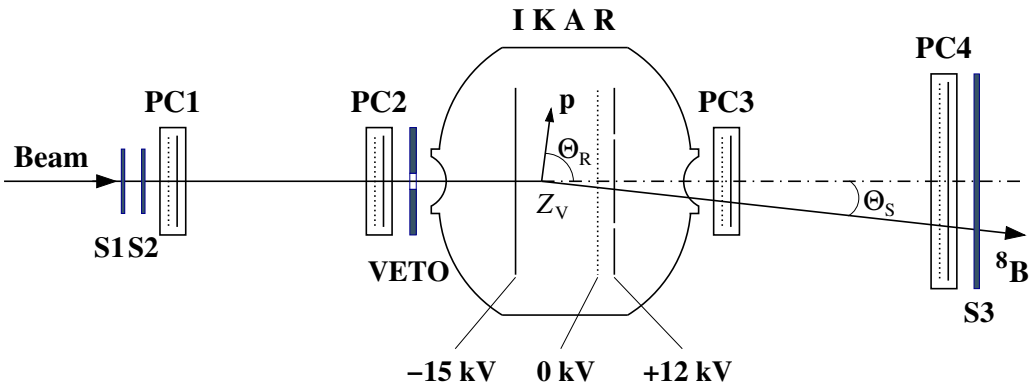

Figure 1: Schematic view of the experimental set-up for small-angle proton elastic scattering on exotic nuclei in inverse kinematics. The hydrogen-filled ionization chamber IKAR serves simultaneously as a gas target and a detector for recoil protons. For the sake of simplicity only one chamber module of six identical ones is shown. The tracking system consisting of four multi-wire proportional chambers PC1–PC4 determines the scattering angle Θ_S of the projectile. Θ_R is the recoil proton scattering angle and Z_V is the vertex point of the interaction. The scintillation counters S1–S3 and VETO are used for beam identification and triggering.

2. Experiment

The experiment was performed at the GSI Darmstadt. A primary ^{22}Ne beam produced by the UNILAC–SIS accelerator complex was focused on an 8 g/cm^2 Be production target at the entrance of the FRagment Separator (FRS). The produced beryllium and boron ions were separated according to their magnetic rigidity and due to their nuclear charge by inserting an achromatic (2.7 g/cm^2) aluminium degrader at the dispersive central focal plane of the FRS. The energy of the secondary beam at the centre of the hydrogen target was 701 MeV/u for ^{7}Be and 702 MeV/u for ^{8}B with an energy spread of 1.3%. The mean energies of the beam particles were determined with an accuracy of about 0.1%. The beam intensity was $\sim 3 \cdot 10^3$ s^{-1}. The contamination from other nuclei was below the 0.1% level.

A schematic view of the experimental layout is displayed in Fig. 1. The main part of the set-up was the ionization chamber IKAR, filled with pure hydrogen at a pressure of 10 bar, which served simultaneously as a gas target and a recoil proton detector. The active target IKAR was developed at PNPI and was originally used in experiments on small-angle hadron elastic scattering [54–57]. The chamber consists of six identical modules. Each module is an axial ionization time-projection chamber consisting of an anode subdivided into a central electrode and a concentric electrode, a cathode and a grid. At the applied high voltages and for the used gas pressure the electron drift time from the cathode to the grid is 23 μs. The signals from the electrodes provide the energy T_R of the recoil proton (or its energy loss in case it leaves the active volume), the scattering angle Θ_R of the recoil proton and the vertex point Z_V of the interaction [49].

Thin α-sources of ^{241}Am were placed on the cathodes and grids, which permitted an energy calibration. The procedure of energy calibration was described in details in Ref. [49]. The energy resolution of IKAR was $\sim$45-55 keV. The α-sources were used also for tracing a small correction which takes into account the limited transparency of the grid and the loss of drifting electrons through adhesion to electronegative impurities in the gas. These losses were continuously controlled by measuring the difference in the positions of two α-peaks corresponding to α-particles emitted from the sources deposited on the grid and on the cathode, respectively [57]. The recoil protons were registered in IKAR in coincidence with the scattered beam particles. For the measurement of the differential cross section dσ/dt, the four-momentum transfer squared t could be determined either from the measured recoil energy T_R, or from the value of the scattering angle Θ_S of the projectiles, which was measured by a tracking detector system consisting of 2 pairs of two-dimensional multi-wire proportional chambers (PC1–PC2 and PC3–PC4) arranged upstream and downstream with respect to IKAR. A set of scintillation counters (S1, S2 and S3) was used for triggering and identification of the beam particles *via* time-of-flight and dE/dx measurements, while a circular-aperture scintillator VETO selected the projectiles which entered IKAR within an area with a diameter of 2 cm around the central

axis. Cylinder bags filled with He gas (not shown in Fig. 1) were placed in between each pair of multi-wire chambers in order to reduce the multiple Coulomb scattering of the projectiles.

A detailed description of the experimental set-up and the procedure of the measurement is presented in Refs. [49–52]. The tracking of the projectiles was accomplished with the same system of multi-wire proportional chambers as in a previous experiment [52]. The corresponding scattering angle $\Theta_{\rm S}$ was calculated using the measured x and y coordinates in the multi-wire proportional chambers. The resolution for the scattering angle was determined by the position resolution and the angular spread due to multiple Coulomb scattering of the projectiles. The total angular resolution was estimated to be $\sigma_\Theta = 0.74$ mrad for the case of ^{7}Be, and $\sigma_\Theta = 1.00$ mrad for ^{8}B, as deduced from calibration measurements with unscattered beam particles.

3. The data analysis

The absolute differential cross section $\mathrm{d}\sigma/\mathrm{d}t$ was determined using the relation

$$\frac{\mathrm{d}\sigma}{\mathrm{d}t} = \frac{\mathrm{d}N}{\mathrm{d}t B n \Delta L} \ . \tag{1}$$

Here, $\mathrm{d}N$ is the number of elastic proton-nucleus scattering events in the interval $\mathrm{d}t$ of the four-momentum transfer squared, B is the corresponding number of beam particles impinging on the target, n is the density of the hydrogen nuclei known from the measured gas pressure and temperature, and ΔL is the effective target length.

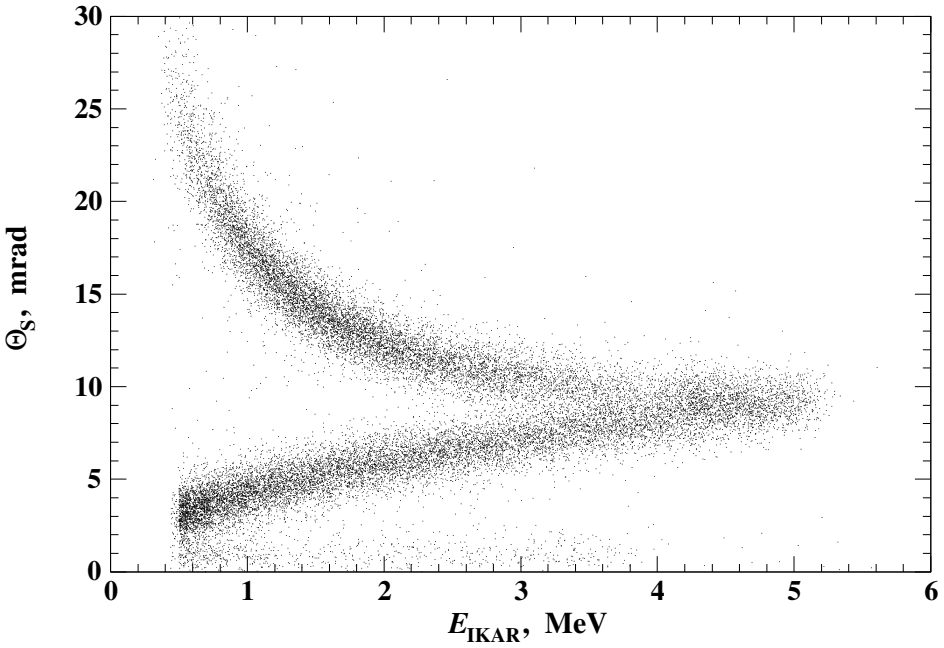

Figure 2: Correlation between the recoil proton energy $E_{\rm IKAR}$ measured in IKAR and the scattering angle $\Theta_{\rm S}$ of the ^{8}B projectile.

For elastic scattering, the value of t can be obtained in two ways, either from the energy $T_{\rm R}$ of the recoil protons as measured in IKAR, according to

$$-t = 2mT_{\rm R} \ , \tag{2}$$

or from the respective projectile scattering angle $\Theta_{\rm S}$ as determined from the tracking detector system, according to

$$-t = 4p_{\rm i}^2 \sin^2 \frac{\Theta_{\rm S}}{2} \left(1 - \frac{E_{\rm i} T_{\rm R}}{p_{\rm i}^2}\right) \approx (p_{\rm i}\Theta_{\rm S})^2 \quad \text{for small } \Theta_{\rm S} \ . \tag{3}$$

Here, m, $p_{\rm i}$, and $E_{\rm i}$ denote the proton mass, the projectile initial momentum and the projectile initial total energy, respectively. Note, that the recoil energy $T_{\rm R}$ is connected to the scattering angle $\Theta_{\rm S}$ by the relation

$$T_{\rm R} = \frac{2p_{\rm i}^2 \sin^2 \frac{\Theta_{\rm S}}{2}}{m + 2E_{\rm i} \sin^2 \frac{\Theta_{\rm S}}{2}} \ . \tag{4}$$

The major stages in the data analysis, such as the t-scale calibration, the determination of the active volume in IKAR, the alignment procedure of the multi-wire proportional chambers, and the selection of the elastic events, were the same as in the previous experiments with IKAR [49, 51, 52]. To reject background events, a correlation between the recoil energy $E_{\rm IKAR}$ deposited in IKAR and the scattering angle $\Theta_{\rm S}$ of the projectile was used (Fig. 2). Note that the ^{8}B nucleus has no particle-stable states. So in selecting elastic p^8B scattering events we had no problem of possible contribution of inelastic scattering. As for p^7Be scattering, according to our calculations, the contribution of scattering with ^{7}Be excitation in our t-range was very small and could be neglected. The calculations of the inelastic cross sections were performed using the eikonal approximation and assuming that the nuclear densities have a Gaussian shape, while the transition densities are those from the Tassie model. In the calculations, all nuclear states below the particle threshold were included with the values of the deformation parameters that are either consistent with the known experimental data or fixed at 0.1. Details of the calculation formalism will be published elsewhere [58].

The recoil proton energy $T_{\rm R}$ was calculated in a fairly large t-range from the measured scattering angles $\Theta_{\rm S}$ according to Eq. (4). In the region of small momentum transfers $|t| \lesssim 0.01$ (GeV/c)^2, where $T_{\rm R} \lesssim 5$ MeV, elastic events correspond to recoil protons stopped within the volume of IKAR. In this case the two ways of calibration of the t-scale, according to Eqs. (2) and (3) gave consistent results. In this t-region, the recoil energy is measured in IKAR with much higher accuracy than the one determined from the scattering angle $\Theta_{\rm S}$ of the projectile using Eq. (4) [49]. Thus, for evaluation of the elastic scattering cross sections $\mathrm{d}\sigma/\mathrm{d}t$, the value t as determined from the energy $E_{\rm IKAR}$ measured in IKAR according to Eq. (2) was favoured. In the region of $|t| \geq 0.01$ (GeV/c)^2 the energy $E_{\rm IKAR}$ is only a part of the total recoil energy $T_{\rm R}$, so the determination of the t-value from the scattering angle $\Theta_{\rm S}$ was more accurate and was consequently preferred. The absolute differential cross section $\mathrm{d}\sigma/\mathrm{d}t$ deduced in the present experiment for proton elastic scattering from the ^{7}Be and ^{8}B isotopes are displayed in Fig. 3 and listed in a tabular form in Appendix A as functions of the four-momentum transfer squared t. The indicated energies $E_{\rm p}$ correspond to the equivalent proton energies in direct kinematics: $E_{\rm p} = (E_{\rm i} - M)m/M$, where M is the mass of the projectile. Only statistical errors are given. A high detection efficiency in the present experiment for the beam particles and the elastic-scattering events in the active target IKAR provide the 2% accuracy of the absolute normalization of the measured cross sections. The uncertainty in the t-scale calibration is estimated to be about 1.5%.

To establish the nuclear density distribution from the measured cross section, the Glauber multiple-scattering theory was applied similarly as in Refs. [48, 50–52]. The differential cross sections for proton elastic scattering on composite targets were calculated as

$$\mathrm{d}\sigma/\mathrm{d}t = (\pi/k^2)\,|F_{\rm el}(\boldsymbol{q})|^2 \tag{5}$$

with the scattering amplitude $F_{\rm el}(\boldsymbol{q})$ given by

$$\begin{aligned} F_{\rm el}(\boldsymbol{q}) &= (\mathrm{i}k/2\pi) \int \mathrm{e}^{\mathrm{i}\boldsymbol{q}\boldsymbol{b}} \{1 - \prod_{\mathrm{i}=1}^{\mathrm{A}} [1 - \gamma_{\rm pN}(\boldsymbol{b} - \boldsymbol{s}_{\rm i})]\} \\ &\times \rho_{\rm A}(\boldsymbol{r}_1, \boldsymbol{r}_2, \ldots, \boldsymbol{r}_{\rm A})\, \mathrm{d}^3\boldsymbol{r}_1\ \mathrm{d}^3\boldsymbol{r}_2 \ldots \mathrm{d}^3\boldsymbol{r}_{\rm A}\ \mathrm{d}^2\boldsymbol{b} \ . \end{aligned} \tag{6}$$

Here $\boldsymbol{q}$ is the momentum transfer ($t = -\boldsymbol{q}^2$), k is the wave number of the incident proton, $\boldsymbol{b}$ stands for the impact vector, $\gamma_{\rm pN}(\boldsymbol{b})$ represent profile functions for the pairwise pN interactions ($N = p, n$), A is

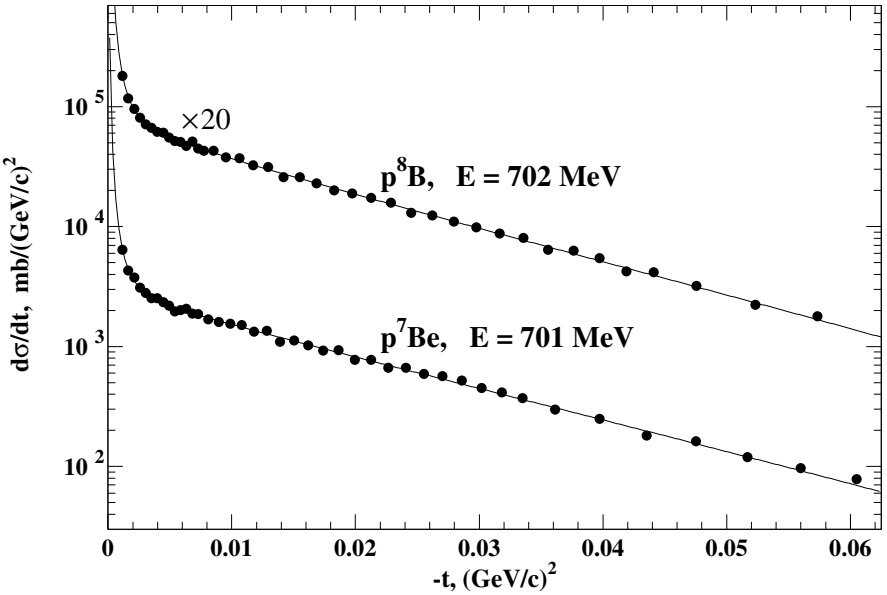

Figure 3: Absolute differential cross sections $\mathrm{d}\sigma/\mathrm{d}t$ for p^7Be and p^8B elastic scattering versus the four-momentum transfer squared. The indicated energies correspond to the equivalent proton energies for direct kinematics. The plotted error bars denote statistical errors only. Solid lines are cross sections calculated within the Glauber theory using the GO parameterization with the fitted parameters.

the nuclear mass number, $\boldsymbol{s}_\mathrm{i}$ $(i = 1, 2, ..., A)$ are the transverse nucleon coordinates $[\boldsymbol{r}_i \equiv (\boldsymbol{s}_i, z_i)]$, and $\rho_\mathrm{A}(\boldsymbol{r}_1, \boldsymbol{r}_2, ..., \boldsymbol{r}_\mathrm{A})$ denotes the nuclear many-body density. The profile functions $\gamma_\mathrm{pN}(\boldsymbol{b})$ are related to the corresponding amplitudes $f_\mathrm{pN}(\boldsymbol{q})$ of free proton-proton (pp) and proton-neutron (pn) scattering by a two-dimensional Fourier transformation. Only the scalar part of the elementary pN scattering amplitude was taken into account, which was described by the high-energy parameterization as

$$f_\mathrm{pN}(\boldsymbol{q}) = (\mathrm{i}k/4\pi)\,\sigma_\mathrm{pN}\;(1\,-\,\mathrm{i}\varepsilon_\mathrm{pN})\;\exp(-\boldsymbol{q}^2\beta_\mathrm{pN}/2)\;, \tag{7}$$

where σ_pp and σ_pn are the total pp and pn cross sections, ε_pp and ε_pn are the ratios of the real to imaginary parts of the amplitudes, and β_pp and β_pn are the slope parameters. The procedure for obtaining the parameters of the free scattering amplitudes is described in detail in Ref. [48]. The values of these parameters which have been taken as inputs into the present analysis are listed in Table 1. In the analysis, the nuclear many-body densities ρ_A were taken as products of the one-body densities, which were parametrized with different functions. The parameters of these densities were determined by fitting the calculated cross-sections to the experimental data similarly as in the previous experiments [48, 50–52].

In the present analysis, four parameterizations of phenomenological nuclear density distributions were applied, labeled as SF (symmetrized Fermi), GH (Gaussian-halo), GG (Gaussian-Gaussian) and GO (Gaussian-oscillator). Each of these parameterizations has two free parameters. In the SF parameterization, the free parameters are the "half density radius" R_0 and the diffuseness parameter a. The corresponding rms matter

Table 1: Values of the free pp and pn amplitudes used in the present analysis of the p^7Be and p^8B elastic scattering cross section. E_p denotes the equivalent proton energy in direct kinematics.

Nucleus	E_p, MeV	σ_pp, mb	σ_pn, mb	ε_pp	ε_pn	$\beta_\mathrm{pp} = \beta_\mathrm{pn}$, fm^2
^{7}Be	701.1	43.48	37.6	0.096	−0.297	0.17
^{8}B	701.8	43.53	37.6	0.095	−0.297	0.17

Table 2: Summary of the parameters obtained by fitting the calculated p^7Be and p^8B elastic scattering cross sections to the measured ones for the parameterizations SF, GH, GG and GO of the nuclear matter density distributions. The presented parameters refer to point-nucleon density distributions. A_n denotes the normalization of the calculated cross section, N is the number of degrees of freedom. A_n, χ^2/N and α are dimensionless, all other fit parameters are given in fm.

Nucleus	Parametrization	χ^2/N	Fit parameters			R_m, fm
			A_n	Density parameters		
^{7}Be	SF	33.1/44	0.97(1)	$R_0 = 1.23(8)$	a = 0.61(2)	2.45(3)
	GH	33.1/44	0.97(1)	$R_m = 2.43(3)$	$\alpha = 0.08(2)$	2.43(3)
	GG	33.3/44	0.97(1)	$R_c = 1.95(4)$	$R_h = 2.94(8)$	2.42(3)
	GO	33.8/44	0.96(1)	$R_c = 1.76(3)$	$R_h = 3.06(6)$	2.40(3)
^{8}B	SF	26.5/39	0.98(1)	$R_0 = 0.96(31)$	a = 0.66(3)	2.57(2)
	GH	25.9/39	0.98(1)	$R_m = 2.56(3)$	$\alpha = 0.10(2)$	2.56(3)
	GG	27.0/39	0.99(1)	$R_c = 2.27(1)$	$R_h = 4.34(28)$	2.62(6)
	GO	25.9/39	0.98(1)	$R_0 = 2.23(1)$	$R_h = 4.33(20)$	2.59(4)

radius R_m is given by

$$R_m = (3/5)^{1/2} R_0 \, [1 + (7/3)(\pi a/R_0)^2]^{1/2} \, . \quad (8)$$

The GH parameterization is determined as a function of the matter radius R_m and the halo parameter α, which varies from 0 to 0.4. The case $\alpha = 0$ corresponds to a Gaussian shape and the one with $\alpha = 0.4$ to a distribution with a pronounced halo component. While the SF and GH parameterizations do not make any difference between core and halo distributions, the GG and GO parameterizations assume that the nuclei consist of core nucleons and valence nucleons with different spatial distributions. The core distribution is assumed to be a Gaussian one in both the GG and GO parameterizations. The valence nucleon density is described by a Gaussian or a $1p$ shell harmonic oscillator-type distribution within the GG or GO parameterization, respectively. The free parameters in the GG and GO parameterizations are the rms radii R_c and R_v (R_h) of the core and valence ("halo") nucleon distributions. It was assumed that ^{8}B consists of a ^{7}Be core and a loosely bound valence proton while ^{7}Be was considered to consist of a ^{4}He core and a "halo" composed of ^{3}He. The explicit expressions for the SF, GH, GG and GO parameterizations are given in Ref. [48].

4. Results on the nuclear matter density distributions and radii

The results of the data analysis with the phenomenological density distribution SF, GH, GG and GO for ^{7}Be and ^{8}B are presented in Table 2. For each density parameterization, the deduced rms nuclear matter radii R_m, the reduced values of χ^2 of the fitting procedure, the values for the fit parameters and the normalization coefficients A_n, with which the calculated cross sections should be multiplied to obtain the same absolute normalization as the experimental ones are presented. For ^{7}Be and ^{8}B, good descriptions of the cross sections have been achieved with all density parameterizations used. The corresponding values of the rms matter radii R_m deduced with all four parameterizations for ^{7}Be and ^{8}B are close to each other, within rather small errors. The values of R_m, averaged over the results obtained with all density parameterizations are:

$$R_m = (2.42 \pm 0.04) \text{ fm} \qquad \text{for } ^7\text{Be},$$
$$R_m = (2.58 \pm 0.06) \text{ fm} \qquad \text{for } ^8\text{B},$$

where the errors include statistical and systematical uncertainties. The systematical errors in R_m appear due to uncertainties in the absolute normalization of the cross sections, in the t-scale calibration, in the parameters of the elementary proton-nucleon scattering amplitudes and due to different model density parameterizations used (for details see Ref. [48]). The mean values for the core and halo radii of ^{8}B deduced

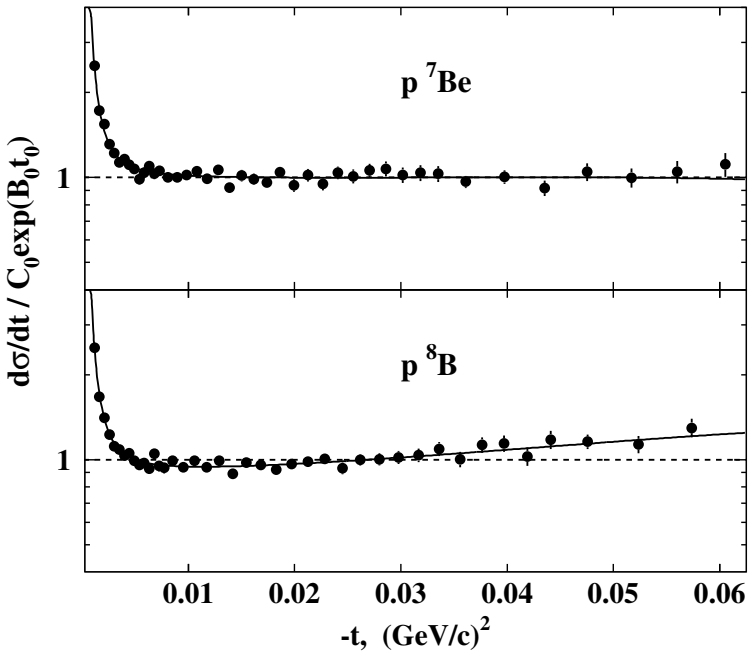

Figure 4: The same cross sections as in Fig 3 but divided by an exponential function. The positive curvature in $\ln(\mathrm{d}\sigma/\mathrm{d}t)$ for ^{8}B is a fingerprint for the halo nature of ^{8}B (for detail see text).

with both the GG and GO parameterizations are $R_\mathrm{c} = 2.25(3)$ fm and $R_\mathrm{h} = 4.24(25)$ fm, respectively. The relation between the rms radii can be written as

$$A{R_\mathrm{m}}^2 = A_\mathrm{c}{R_\mathrm{c}}^2 + A_\mathrm{h}{R_\mathrm{h}}^2 \ . \tag{9}$$

The solid lines in Fig. 3 represent the results of the $\mathrm{d}\sigma/\mathrm{d}t$ using the GO parameterization. At $|t| < 0.005$ $(\mathrm{GeV}/c)^2$ the steep rise of the cross section with decreasing $|t|$ is caused by Coulomb scattering. The behaviour of the measured curvature of the differential cross section at $0.005 < |t| < 0.06$ $(\mathrm{GeV}/c)^2$ is an indication of the halo occurrence (for details see Refs. [48, 51, 53]). This curvature can be better seen if one plots the cross section divided by the exponential function $C_0 \cdot \exp(B_0 t)$, where B_0 and C_0 are the slope and absolute values of the nuclear part of the differential cross section calculated at $|t| = 0.01$ $(\mathrm{GeV}/c)^2$. Such a plot is presented in Fig. 4 for ^{7}Be and ^{8}B using the GO parameterization. As it was shown in [48, 51], the halo nuclei demonstrate a positive curvature in the t-dependence of $\ln(\mathrm{d}\sigma/\mathrm{d}t)$. This may be explained by the fact that contributions to the cross section for proton scattering from the core and from the halo of these nuclei exhibit a different angular dependence. The contribution to the cross section from the scattering on the halo proton decreases faster with increasing $|t|$ than the one from scattering on the core nucleons. In Fig. 4 the best fit to the experimental data in the case of ^{8}B corresponds to the curve with $R_\mathrm{v} = 4.24$ fm and demonstrates a positive curvature (at $0.01 < |t| < 0.03$ $(\mathrm{GeV}/c)^2$). This positive curvature in $\ln(\mathrm{d}\sigma/\mathrm{d}t)$ for ^{8}B is an indication of a halo structure. No such positive curvature is observed for ^{7}Be.

The core and nuclear matter distributions deduced for ^{8}B by using different parameterizations of the nuclear matter distributions are compared in Fig. 5 with the nuclear matter distribution for ^{7}Be. All density distributions refer to point nucleon distributions. Note, that the description of the nuclear matter density distribution for all four parameterizations used are rather similar in the case of ^{7}Be as well as in the case of ^{8}B. The deduced rms matter radii R_m are practically the same for the four versions of the analysis. All versions also resemble each other in reproducing an extended nuclear matter distribution in ^{8}B.

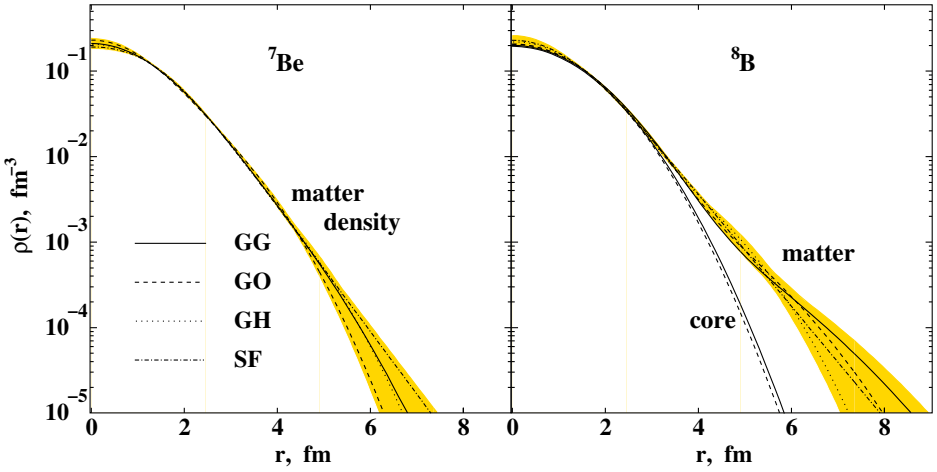

Figure 5: Nuclear matter density distributions for ^{7}Be and ^{8}B deduced from the experimental data. In the data analysis, the ^{8}B nucleus was assumed to consist of a ^{7}Be core and a loosely bound valence proton. The error-band represents the envelopes of the density variation within the model parameterization applied, superimposed by the statistical errors. The results for all parameterizations used in the description of nuclear matter densities are rather similar and demonstrate a clear evidence for the existence of a proton halo in ^{8}B. The deduced core radius in ^{8}B is smaller than the ^{7}Be matter radius in accordance with the theoretical prediction of Grigorenko et al. [33].

5. Discussion

The value of $R_{\rm m} = 2.42(4)$ fm for ^{7}Be derived in this work coincides within the errors with the result of Warner et al. [38], but exceeds essentially the value of $R_{\rm m} = 2.31(2)$ fm obtained by Tanihata *et al.* [21]. A comparison of the rms radii $R_{\rm m}$ and $R_{\rm p}$ calculated using different theoretical models together with the experimental values is presented in Table 3. The $R_{\rm m}$ value from the present experiment agrees within the error limits with most of the theoretical results. Note, that the best agreement with theoretical calculations is obtained in cases when the experimental value of $R_{\rm p}$ [39, 40] measured with a high precision also coincides with the theoretical ones [34, 43]. The value of $R_{\rm p}$ derived from an interaction cross section measurement [21] is model dependent and is much smaller than that obtained in the laser spectroscopy measurement [39, 40]. By combining the matter radius $R_{\rm m}$, deduced in the present work for ^{7}Be, with $R_{\rm p}$ [39, 40] and using the expression

$$A{R_{\rm m}}^2 = Z{R_{\rm p}}^2 + N{R_{\rm n}}^2 \ , \tag{10}$$

where Z and N are the numbers of protons and neutrons, the rms neutron radius for ^{7}Be was determined to be

$$R_{\rm n} = (2.27 \pm 0.10) \text{ fm}.$$

For the thickness of the proton skin $\delta_{\rm pn} = R_{\rm p} - R_{\rm n}$, we deduced the value of $\delta_{\rm pn} = 0.23(10)$ fm. This result is an indication of a noticeable proton skin in ^{7}Be.

A summary of the results on the structure of the proton-rich ^{8}B nucleus obtained from experimental and theoretical research is presented in Table 4. The experimental value of $R_{\rm m} = 2.58(6)$ fm, deduced in the present work, is in good agreement with the value of $R_{\rm m} = 2.61(8)$ fm obtained with the modified Glauber model approach in the recent analysis [25] of all existing data for reaction cross sections but is larger than that of earlier results of Refs. [21] and [24]. Our value of $R_{\rm m}$ turns out to be within the experimental errors in almost perfect agreement with many theoretical results [11, 31, 33, 35] presented in Table 4. In some theoretical studies the nucleon structure of ^{8}B was treated as a three-cluster system [11, 26, 31, 33]. In particular, the theoretical description of ^{8}B in Ref. [33] is performed assuming (^{4}He + ^{3}He + p) three-body model with explicit inclusion of the binary (^{7}Be + p) channel. The model describes the bulk properties of ^{8}B well and predicts a value of $R_{\rm m} = 2.59$ fm. The model also reproduces the experimental data [16] on the

Table 3: Comparison of the calculated rms radii of the nuclear matter and the proton densities with the experimental values for ^{7}Be.

	R_m, (fm)	R_p, (fm)	Reference	
Experiment	**2.42(4)**	–	**this work**[a]	
	2.31 (2)	2.36 (2)	Tanihata 1988	[21][b]
	2.36 (6)	–	Warner 2001	[38][c]
	–	2.507 (17)	Nörtershäuser 2009	[40][d]
Theory	2.43	2.48	Csótó 1993	[11][e]
	2.36	2.41	Varga 1995	[31][e]
	2.420	2.549	Fayans 1995	[32][f]
	2.50	2.64	Shen 1996	[41][g]
	2.280	2.369	Negoita 1996	[15][g]
	2.37–2.40	–	Grigorenko 1998	[33][e]
	2.413	2.525	Patra 1998	[34][h]
	2.49	2.63	Dhiman 2005	[35][g]
	2.327	2.455	Wang 2009	[36][h]
	2.37	2.45	Krieger 2012	[42][i]
	2.39	2.47	Pastore 2013	[37][j]
	2.43	2.51	Carlson 2015	[43][i]

[a] elastic proton scattering
[b] interaction cross section measurements
[c] reaction cross section measurements
[d] laser spectroscopy measurements
[e] microscopic cluster model
[f] semi-microscopic folding calculations
[g] Skirme-Hartree-Fock (SkHF) model
[h] Relativistic Mean Field (RMF) model
[i] Fermionic Molecular Dynamics (FMD) calculations
[j] Green's function Monte Carlo (GFMC) calculations

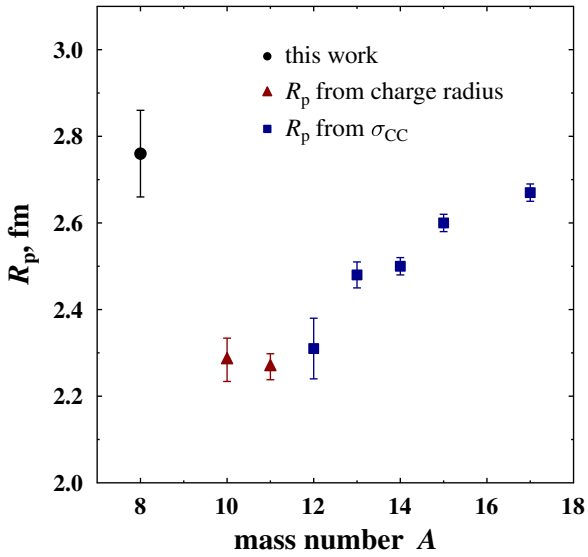

Figure 6: Experimental rms proton radii R_p for the boron isotopes. The filled circle is the result of the present work. The filled triangles are values of R_p for ^{10}B and ^{11}B determined from measured charge radii from Ref. [62]. The squares are proton radii R_p deduced from measured charge-changing cross sections using a finite-range Glauber model analysis [63].

shape and a rather narrow width of the momentum distribution of the ^{7}Be fragments in the proton removal channel of the ^{8}B high-energy break-up. An important finding of this model [33] is that the presence of a loosely bound proton leads to a contraction of the ^{7}Be cluster inside ^{8}B. Indeed, according to our measurements, the deduced ^{7}Be core of the ^{8}B nucleus $R_c = 2.25(3)$ fm is essentially smaller than the ^{7}Be matter radius $R_m = 2.42(4)$ fm.

The rms halo radius $R_h = 4.24(25)$ fm derived in the present experiment confirms the halo nature of ^{8}B and can be compared with the values obtained in other works (Table 5). Experimental results presented there include measurements of the nuclear asymptotic normalization coefficient (ANC) which permits to extract the halo radius [59–61] and the model-dependent analysis of the break-up cross section [15]. Several theoretical calculations [14, 27, 33, 36] are also presented in Table 5. The present value of the halo radius R_h agrees within the error limits with the results of all investigations displayed in Table 5.

A criterion for a quantitative assessment of halo nuclei was proposed in Ref. [33]. The ratio of the valence nucleon to the core nucleon radii $\kappa = R_v/R_c$ is used as a gauge for the halo existence. For light nuclei close to the valley of beta stability, theory predicts typically $\kappa \approx 1.20-1.25$, while for the halo structure this value can be essentially larger, up to $\kappa > 2$ [2]. In the three-cluster model [33] a value of $\kappa = 1.75$ was obtained for ^{8}B which can be compared with $\kappa = 1.88(14)$ deduced from the present measurement. In previous experiments on proton elastic scattering with the same method [48, 52] we obtained for the neutron halo nuclei ^{6}He and ^{14}Be the values of $\kappa = 1.76$ and $\kappa = 1.91$, respectively, values which are close to that for ^{8}B.

Under the assumption that for ^{8}B the rms radius of the neutron distribution R_n equals the core radius R_c and using expression (10) we obtain the rms radius of the proton distribution in ^{8}B as

$$R_p = (2.76 \pm 0.09) \text{ fm}.$$

The results on R_p (and R_n) for ^{8}B for other experimental and theoretical investigations are presented in Table 4. The values indicated as experimental are model dependent and are widely scattered. The present result is in agreement with some of the theoretical calculations [11, 31, 33, 35]. In Fig. 6, the value of

Table 4: Summary of the results obtained for ^{8}B from experimental and theoretical studies. The values R_m, R_p and R_n denote the rms radii of the nuclear matter, and of the proton and neutron distributions, respectively.

	R_m, (fm)	R_p, (fm)	R_n, (fm)	Reference	
Experiment	**2.58 (6)**	**2.76 (9)**	**2.25 (3)**	**this work**[a]	
	2.38 (4)	2.45 (5)	2.27 (4)	Tanihata 1988	[21][b]
	2.43 (3)	2.49 (3)	2.33 (3)	Obuti 1996	[24][b]
	2.50 (4)	–	–	Al-Khalili 1996	[23][c]
	2.55 (8)	2.76 (8)	2.16 (3)	Negoita 1996	[15][d]
	2.45(10)	2.53 (13)	2.31 (5)	Fukuda 1999	[19][c]
	2.61 (8)	–	–	Fan 2015	[25][e]
Theory	2.71	2.98	2.20	Minamisono 1992	[10][f]
	2.57	2.74	2.25	Csótó 1993	[11][g]
	2.73	2.88	2.46	Baye 1994	[26][g]
	2.56	2.73	2.24	Varga 1995	[31][g]
	2.507	2.68	2.19	Fayans 1995	[32][h]
	2.68	2.92	2.21	Brown 1996	[27][f]
	2.59	2.75	2.30	Grigorenko 1998	[33][g]
	2.494	2.654	2.202	Patra 1998	[34][j]
	2.627	2.861	2.181	Kitagawa 1999	[28][f]
	2.57	2.73	2.27	Dhiman 2005	[35][i]
	2.50	2.64	2.24	Furutachi 2009	[29][k]
	2.367	2.537	2.052	Wang 2009	[36][j]
	2.35	2.48	2.11	Pastore 2013	[37][l]
	2.262	2.373	2.062	Henninger 2015	[30][m]

[a] elastic proton scattering
[b] Glauber-model analysis of the interaction cross section
[c] Glauber-model analysis of the reaction cross section
[d] analysis of the break-up and reaction cross sections
[e] modified Glauber model used in the analysis of existing reaction cross sections
[f] shell model
[g] microscopic cluster model
[h] semi-microscopic folding calculations
[i] Skirme-Hartree-Fock (SkHF) model
[j] Relativistic Mean Field (RMF) model
[k] an extended framework based on antisymmetrized molecular dynamics (MAMD)
[l] Green's function Monte Carlo (GFMC) calculations
[m] Fermionic Molecular Dynamics (FMD) calculations

$R_{\rm p}$ for ^{8}B determined in the present work is compared with the existing experimental data on $R_{\rm p}$ values for other boron isotopes. The weighted average charge radii $R_{\rm ch} = 2.43(5)$ fm and $R_{\rm ch} = 2.41(3)$ fm for the stable ^{10}B and ^{11}B are known from electron and π^+ scattering measurements and from muonic atom X-rays studies [62]. Taking into account the relation between the point proton and the charge radius of a nucleus [39], the corresponding proton radii are deduced to be $R_{\rm p} = 2.28(5)$ fm for ^{10}B and $R_{\rm p} = 2.27(3)$ fm for ^{11}B, respectively. The values $R_{\rm p}$ for the neutron-rich boron isotopes $^{12-17}$B were recently determined from charge-changing cross section measurements at GSI [63]. The value of $R_{\rm p}$ for ^{8}B determined in our work is fairly larger than those of nuclei of the stable isotopes ^{10}B and ^{11}B, which confirms the existence of a halo in ^{8}B. Using the determined value of $R_{\rm p}$ we also deduce the charge radius for ^{8}B as $R_{\rm ch} = 2.89(9)$ fm. Finally, for the thickness of the proton skin $\delta_{\rm pn} = R_{\rm p} - R_{\rm n}$ for ^{8}B we obtain a value of $\delta_{\rm pn} = 0.51(9)$ fm. This value seems to be the largest one in comparison with other measured values of $\delta_{\rm pn}$ for proton-rich nuclei [64].

The present measurements of the nuclear matter radius $R_{\rm m}$ and the charge radius $R_{\rm ch}$ for ^{8}B as well as $R_{\rm m}$ for ^{7}Be may be important for nuclear astrophysics because these quantities are correlated to the astrophysical factor S_{17} for the radioactive proton capture on ^{7}Be at low energies [9, 65]. Since such correlations are model dependent, the results of the present measurements may also be used as a check of validity of the $S_{17}(0)$ calculation. The structure of ^{8}B obtained in the present experiment is in good agreement with the results of the theoretical study in Refs [33, 35] where the authors predict the S-factor values of $S_{17}(0) = 19.2$ eVb and $S_{17}(0) = 22.0$ eVb, respectively. These values are consistent with the Solar Fusion II recomendation [7]

$$S_{17}(0) = 20.8 \pm 0.7(\text{expt}) \pm 1.4(\text{theor}) \text{ eVb}$$

based on an extrapolation of experimental data for $S_{17}(E)$.

6. Summary

In the present work we used a method, developed by PNPI–GSI collaboration, of small angle proton-nucleus elastic scattering in inverse kinematics to determine the nuclear matter density distribution of the proton-rich ^{7}Be and ^{8}B nuclei. The absolute differential cross sections for proton elastic scattering was measured in the ranges $0.001 \leqslant |t| \leqslant 0.08$ $(\text{GeV}/c)^2$ and $0.001 \leqslant |t| \leqslant 0.06$ $(\text{GeV}/c)^2$, of the four-momentum transfer squared for p^{7}Be and p^{8}B scattering, respectively. The cross sections were determined using secondary beams from the GSI fragment separator FRS at an energy of ~ 700 MeV/nucleon. The hydrogen-filled ionization chamber IKAR served simultaneously as a hydrogen target and a recoil-proton detector. The nuclear matter radii and radial matter distributions were determined with the aid of the Glauber multiple-scattering theory. In the analysis, four phenomenological parameterizations of the nuclear density distributions were used, each of these parameterizations had two free parameters. For both investigated nuclei, a good description of the cross sections was obtained with all the used density parameterizations. The

Table 5: Experimental and theoretical values of the rms halo radius $R_{\rm h}$ in ^{8}B.

$R_{\rm h}$, (fm)	Reference		
4.62 (24)	Carstoiu 2007	[61]	measurement of the asymptotic normalization coefficient (ANC)
4.44	Brown 1996	[27]	shell-model calculations
4.24	Kelley 1996	[14]	single-particle Hamiltonian model
4.24 (25)	**This work**		elastic proton scattering
4.20 (22)	Carstoiu 2001	[59]	measurement of the ANC
4.03	Grigorenko 1998	[33]	cluster model
3.98	Wang 2009	[36]	ANC method in RMF theory
3.97 (12)	Negoita 1996	[15]	model-dependent break-up cross section analysis
3.90 (20)	Liu 2004	[60]	measurement of the ANC

value of $R_{\rm m} = 2.42(4)$ fm deduced for ^{7}Be is larger than the matter radii obtained in previous experiments based on measurements of the total interaction [21] and reaction [38] cross sections. On the other hand, our $R_{\rm m}$ value is in perfect agreement with most of the theoretical predictions (Table 3). A noticeable proton skin $\delta_{\rm pn} = 0.23(10)$ fm was obtained by combining the value $R_{\rm m}$ with the proton radius $R_{\rm p}$ measured by a laser spectroscopy technique [39, 40]. Similar matter density distributions were determined using the all four parameterizations.

The nuclear matter density distributions deduced for the proton-rich ^{8}B nucleus are also very similar for all the parameterizations used and demonstrate an extended distribution. In the case of the GG and GO parameterizations, the deduced rms halo radius $R_{\rm h} = 4.24(25)$ fm is 1.88 times larger than the rms core radius $R_{\rm c} = 2.25(3)$ fm, thus giving clear evidence of a halo structure. The value of $R_{\rm h}$ is in good agreement with the existing experimental measurements and theoretical calculations (Table 5). The nuclear matter radius $R_{\rm m} = 2.58(6)$ fm deduced in this work is in perfect agreement with the recent experimental result of Fan *et al.* [25], where $R_{\rm m}$ was obtained from the existing data on reaction cross-sections using a modified Glauber model, and in agreement with several theoretical calculations [11, 31, 33, 35] (Table 4). In the three-body model, Grigorenko *et al.* [33] predicted a contraction of the ^{7}Be cluster inside ^{8}B. The present measurement supports this finding. Assuming that the rms radius of the neutron distribution $R_{\rm n}$ for ^{8}B is equal to the core radius $R_{\rm c}$, we have deduced the rms radius of the proton distribution as $R_{\rm p} = 2.76(9)$ fm. This value is in agreement with theoretical calculations (the same as in the case of $R_{\rm m}$) and is significantly larger than the $R_{\rm p}$ values for the neighboring successive boron isotopes (Fig. 6). It should also be stated that the proton skin in ^{8}B is the largest one observed up to now.

The results of the present work on the structure of ^{8}B and ^{7}Be may be important for nuclear astrophysics in calculation of the ^{7}Be$(p,\gamma)^8$B astrophysical S-factor at zero energy.

Acknowledgements

The authors are grateful to A. Bleile, G. Ickert, A.Brünle, K.-H. Behr and W. Niebur for their technical assistance in the preparation of the experimental set-up. The visiting group from PNPI thanks the GSI authorities for the hospitality.

References

[1] I. Tanihata, H. Savajols, R. Kanungo, Prog. Part. Nucl. Phys. 68 (2013) 215.
[2] B. Jonson, Phys. Rep. 389 (2004) 1.
[3] A. Ozawa, T. Suzuki, I. Tanihata, Nucl. Phys. A 693 (2001) 3.
[4] I. Tanihata, J. Phys. G 22 (1996) 1.
[5] M. Wang, G. Audi, A. Wapstra, F. Kondev, M. MacCormick, X. Xu, B. Pfeiffer, Chin. Phys. C 36 (2012) 1603.
[6] J. Bahcall, W. Huebner, S. Lubow, P. Parker, R. Ulrich, Rev. Mod. Phys. 54 (1982) 767.
[7] E. Adelberger, A. Garcia, R. H. Robertson, K. Snover, A. Balantekin, K. Heeger, M. Ramsey-Musolf, D. Bemmerer, A. Junghans, C. Bertulani, J.-W. Chen, H. Costantini, P. Prati, M. Couder, E. Uberseder, M. Wiescher, R. Cyburt, B. Davids, S. Freedman, M. Gai, D. Gazit, L. Gialanella, G. Imbriani, U. Greife, M. Hass, W. Haxton, T. Itahashi, K. Kubodera, K. Langanke, D. Leitner, M. Leitner, P. Vetter, L. Winslow, L. Marcucci, T. Motobayashi, A. Mukhamedzhanov, R. Tribble, K. M. Nollet, F. Nunes, T.-S. Park, P. Parker, R. Shiavilla, E. Simpson, C. Spitaleri, F. Strieder, H.-P. Trautvetter, K. Suemmerer, S. Typel, Rev. Mod. Phys. 83 (2011) 195.
[8] K. Riisager, A. Jensen, Phys. Lett. B 301 (1993) 6.
[9] A. Csótó, K. Langanke, Nucl. Phys. A 636 (1998) 240.
[10] T. Minamisono, T. Ohtsubo, I. Minami, S. Fukuda, A. Kitagawa, M. Fukuda, K. Matsuta, Y. Nojiri, S. Takeda, H. Sagawa, H. Kitagawa, Phys. Rev. Lett. 69 (1992) 2058.
[11] A. Csótó, Phys. Lett. B 315 (1993) 24.
[12] H. Nakada, T. Otsuka, Phys. Rev. C 49 (1994) 886.
[13] W. Schwab, H. Geissel, H. Lenske, K.-H. Behr, A. Brünle, K. Burkard, H. Irnich, T. Kobayashi, G. Kraus, A. Magel, G. Münzenberg, F. Nickel, K. Riisager, C. Scheidenberger, B. Sherrill, T. Suzuki, B. Voss, Z. Phys. A 350 (1995) 283.
[14] J. Kelley, S. Austin, A. Azhari, D. Bazin, J. Brown, H. Esbensen, M. Fauerbach, M. Hellström, S. Hirzebruch, R. Kryger, D. Morrissey, R. Pfaff, C. Powell, E. Ramakrishnan, B. Sherrill, M. Steiner, T. Suomijärvi, M. Thoennessen, Phys. Rev. Lett. 77 (1996) 5020.
[15] F. Negoita, C. Borcea, F. Carstoiu, M. Lewitowicz, M. Saint-Laurent, R. Anne, D. Bazin, J. Corre, P. Roussel-Chomaz, V. Borrel, D. Guillemaud-Mueller, H. Keller, A. Mueller, F. Pougheon, O. Sorlin, S. Lukyanov, Y. Penionzhkevich, A. Fomichev, N. Skobelev, O. Tarasov, Z. Dlouhy, A. Kordyasz, Phys. Rev. C 54 (1996) 1787.

[16] M. Smedberg, T. Baumann, T. Aumann, L. Axelsson, U. Bergmann, M. Borge, D. Cortina-Gil, L. Fraile, H. Geissel, L. Grigorenko, M. Hellström, M. Ivanov, N. Iwasa, R. Janik, B. Jonson, H. Lenske, K. Markenroth, G. Münzenberg, T. Nilsson, A. Richter, K. Riisager, C. Scheidenberger, G. Schrieder, W. Schwab, H. Simon, B. Sitar, P. Strmen, K. Sümmerer, M. Winkler, M. Zhukov, Phys. Lett. B 452 (1999) 1.
[17] D. Cortina-Gil, J. Fernandez-Vazquez, F. Attallah, T. Baumann, J. Benlliure, M. Borge, L. Culkov, C. Forssén, L. Fraile, H. Geissel, J. Gerl, K. Itahashi, R. Janik, B. Jonson, S. Karlsson, H. Lenske, S. Mandal, K. Markenroth, M. Meister, M. Mocko, G. Münzenberg, T. Ohtsubo, A. Ozawa, Y. Parfenova, V. Pribora, A. Richter, K. Riisager, R. Schneider, H. Scheit, G. Schrieder, N. Shulgina, H. Simon, B. Sitar, A. Stolz, P. Strmen, K. Sümmerer, I. Szarka, S. Wan, H. Weick, M. Zhukov, Nucl. Phys. A 720 (2003) 3.
[18] B. Blank, C. Marchand, M. Primakoff, T. Baumann, F. Boué, H. Geissel, M. Hellström, N. Iwasa, W. Schwab, K. Sümmerer, M. Gai, Nucl. Phys. A 624 (1997) 242.
[19] M. Fukuda, M. Mihara, T. Fukao, S. Fukuda, M. Ishihara, S. Ito, T. Kobayashi, K. Matsuta, T. Minamisono, S. Momota, T. Nakamura, Y. Nojiri, Y. Ogawa, T. Ohtsubo, T. Onishi, A. Ozawa, T. Suzuki, M. Tanigaki, I. Tanihata, K. Yoshida, Nucl. Phys. A 656 (1999) 209.
[20] R. Warner, F. Becchetti, J. Brown, A. Galonsky, J. Kelley, A. Nadsen, R. Ronningen, J. Tostevin, J. Winfield, P. Zecher, Phys. Rev. C 69 (2004) 024612.
[21] I. Tanihata, T. Kobayashi, O. Yamakawa, S. Shimoura, K. Ekuni, K. Sugimoto, N. Takahashi, T. Shimoda, H. Sato, Phys. Lett. B 206 (1988) 592.
[22] R. Warner, J. Kelley, P. Zecher, F. Becchetti, J. Brown, C. Carpenter, A. Galonsky, B. Sherrill, J. Wang, J. Winfield, Phys. Rev. C 52 (1995) R1166.
[23] J. Al-Khalili, J. Tostevin, Phys. Rev. Lett. 76 (1996) 3903.
[24] M. Obuti, T. Kobayashi, D. Hirata, Y. Ogawa, A. Ozawa, K. Sugimoto, I. Tanihata, D. Olson, W. Christie, H. Wieman, Nucl. Phys. A 609 (1996) 74.
[25] G. Fan, M. Fukuda, D. Nishimura, X. Cai, S. Fukuda, I. Hachiuma, C. Ichikawa, T. Izumikawa, M. Kanazawa, A. Kitagawa, T. Kuboki, M. Lantz, M. Mihara, M. Nagashima, K. Namihira, Y. Ohkuma, T. Ohtsubo, Z. Ren, S. Sato, Z. Sheng, M. Sugiyama, S. Suzuki, T. Suzuki, M. Takechi, T. Yamaguchi, W. Xu, Phys. Rev. C 91 (2015) 014614.
[26] D. Baye, P. Descouvemont, N. Timofeyuk, Nucl. Phys. A 577 (1994) 624.
[27] B. Brown, A. Csótó, R. Sherr, Nucl. Phys. A 597 (1996) 66.
[28] H. Kitagawa, Progr. Theor. Phys. 102 (1999) 1015.
[29] N. Furutachi, M. Kimura, A. Doté, Y. Kanada-En'yo, Progr. Theor. Phys. 122 (2009) 865.
[30] K. Henninger, T. Neff, H. Feldmeier, J. Phys.: Conf. Ser. 599 (2015) 012038.
[31] K. Varga, Y. Suzuki, I. Tanihata, Phys. Rev. C 52 (1995) 3013.
[32] S. Fayans, O. Knyazkov, I. Kuchtina, Y. Penionzhkevich, N. Skobelev, Phys. Lett. B 357 (1995) 509.
[33] L. Grigorenko, B. Danilin, V. Efros, N. Shuĺgina, M. Zhukov, Phys. Rev. C 57 (1998) 2099(R).
[34] S. Patra, C.-L. Wu, C. Praharaj, Mod. Phys. Lett. A 13 (1998) 2743.
[35] S. Dhiman, R. Shyam, J. Phys. G: Nucl. Part. Phys. 31 (2005) S1531.
[36] C. Wang, T. Dong, Z. Zhu, Z. Ren, Mod. Phys. Lett. A 24 (2009) 1453.
[37] S. Pastore, S. Pieper, R. Schiavilla, R. Wiringa, Phys. Rev. C 87 (2013) 035503.
[38] R. Warner, M. McKinnon, J. Needleman, N. Shaner, F. Becchetti, D. Roberts, A. Galonsky, R. Ronningen, M. Steiner, J. Brown, J. Kolata, A. Nadsen, K. Subotic, Phys. Rev. C 64 (2001) 044611.
[39] Z.-T. Lu, P. Mueller, G. F. Drake, W. Nortershäuser, S. Pieper, Z.-C. Yan, Rev. Mod. Phys. 85 (2013) 1383.
[40] W. Nörtershäuser, D. Tiedemann, M. Žáková, Z. Andjelkovic, K. Blaum, M. Bissell, R. Cazan, G. Drake, C. Geppert, M. Kowalska, J. Krämer, A. Krieger, R. Neugart, R. Sánchez, F. Schmidt-Kaler, Z.-C. Yan, D. Yordanov, C. Zimmermann, Phys. Rev. Lett. 102 (2009) 062503.
[41] Y. Shen, Z. Ren, Phys. Rev. C 54 (1996) 1158.
[42] A. Krieger, K. Blaum, M. Bissell, N. Frömmgen, C. Geppert, M. Hammen, K. Kreim, M. Kowalska, J. Krämer, T. Neff, R. Neugart, G. Neyens, W. Nortershäuser, C. Novotny, R. Sánchez, D. Yordanov, Phys. Rev. Lett. 108 (2012) 142501.
[43] J. Carlson, F. Gandolfi, F. Pederiva, S. Pieper, R. Schiavilla, K. Schmidt, R. Wiringa, Rev. Mod. Phys. 87 (2015) 1067.
[44] G. Alkhazov, S. Belostotsky, A. Vorobyov, Phys. Rep. 42C (1978) 89.
[45] H. Sakaguchi, J. Zenihiro, Prog. Part. Nucl. Phys. 97 (2017) 1.
[46] G. Alkhazov, A. Lobodenko, JETP Lett. 55 (1992) 379.
[47] G. Alkhazov, M. Andronenko, A. Dobrovolsky, P. Egelhof, G. Gavrilov, H. Geissel, H. Irnich, A. Khanzadeev, G. Korolev, A. Lobodenko, G. Münzenberg, M. Mutterer, S. Neumaier, F. Nickel, W. Schwab, D. Seliverstov, T. Suzuki, J. Theobald, N. Timofeev, A. Vorobyov, V. Yatsoura, Phys. Rev. Lett. 78 (1997) 2313.
[48] G. Alkhazov, A. Dobrovolsky, P. Egelhof, H. Geissel, H. Irnich, A. Khanzadeev, G. Korolev, A. Lobodenko, G. Münzenberg, M. Mutterer, S. Neumaier, W. Schwab, D. Seliverstov, T. Suzuki, A. Vorobyov, Nucl. Phys. A 712 (2002) 269.
[49] S. Neumaier, G. Alkhazov, M. Andronenko, A. Dobrovolsky, P. Egelhof, G. Gavrilov, H. Geissel, H. Irnich, A. Khanzadeev, G. Korolev, A. Lobodenko, G. Münzenberg, M. Mutterer, W. Schwab, D. Seliverstov, T. Suzuki, N. Timofeev, A. Vorobyov, V. Yatsoura, Nucl. Phys. A 712 (2002) 247.
[50] P. Egelhof, G. Alkhazov, M. Andronenko, A. Bauchet, A. Dobrovolsky, S. Fritz, G. Gavrilov, H. Geissel, C. Gross, A. Khanzadeev, G. Korolev, G. Kraus, A. Lobodenko, G. Münzenberg, M. Mutterer, S. Neumaier, T. Schäfer, C. Scheidenberger, D. Seliverstov, N. Timofeev, A. Vorobyov, V. Yatsoura, Eur. Phys. J. A 15 (2002) 27.
[51] A. Dobrovolsky, G. Alkhazov, M. Andronenko, A. Bauchet, P. Egelhof, S. Fritz, H. Geissel, C. Gross, A. Khanzadeev, G. Korolev, G. Kraus, A. Lobodenko, G. Münzenberg, M. Mutterer, S. Neumaier, T. Schäfer, C. Scheidenberger, D. Seliverstov, N. Timofeev, A. Vorobyov, V. Yatsoura, Nucl. Phys. A 766 (2006) 1.

[52] S. Ilieva, F. Aksouh, G. Alkhazov, L. Chulkov, A. Dobrovolsky, P. Egelhof, H. Geissel, M. Gorska, A. Inglessi, R. Kanungo, A. Khanzadeev, O. Kiselev, G. Korolev, X. Le, Y. Litvinov, C. Nociforo, D. Seliverstov, L. Sergeev, H. Simon, V. Volkov, A. Vorobyov, H. Weick, V. Yatsoura, A. Zhdanov, Nucl. Phys. A 875 (2012) 8.
[53] G. Korolev, A. Dobrovolsky, A. Inglessi, G. Alkhazov, P. Egelhof, A. Estradé, I. Dillmann, F. Farinon, H. Geissel, S. Ilieva, Y.Ke, A. Khanzadeev, O. Kiselev, J. Kurcewicz, X. Le, Y. Litvinov, G. Petrov, A. Prochazka, C. Scheidenberger, L. Sergeev, H. Simon, M.Takechi, S. Tang, V. Volkov, A. Vorobyov, H. Weick, V. Yatsoura, Phys. Letters B 780 (2018) 200.
[54] A. Vorobyov, G. Korolev, V. Schegelsky, G. Solyakin, G. Sokolov, Y. Zalite, Nucl. Instr. Meth. 119 (1974) 509.
[55] A. Vorobyov, Y. Grigorev, Y. Zalite, G. Korolev, E. Maev, G. Sokolov, A. Khanzadeev, Instrum. Exp. Tech. 24 (1982) 1127.
[56] J. Burq, M. Chemarin, M. Chevallier, A. Denisov, C. Doré, T. Ekelöf, P. Grafström, E. Hagberg, B. Ille, A. Kashchuk, G. Korolev, S. Kullander, M. Lambert, J. Martin, S. Maury, J. Paumier, M. Querrou, V. Schegelsky, E. Spiridenkov, I. Tkach, A. Vorobyov, Phys. Lett. B 77 (1978) 438.
[57] J. Burq, M. Chemarin, M. Chevallier, A. Denisov, C. Doré, T. Ekelöf, J.Fay, P. Grafström, L. Gustafsson, E. Hagberg, B. Ille, A. Kashchuk, G. Korolev, A. Kulikov, S. Kullander, M. Lambert, J. Martin, S. Maury, M. Querrou, V. Schegelsky, E. Spiridenkov, I. Tkach, M. Verbeken, A. Vorobyov, Nucl. Phys. B (1983) 285.
[58] G. Colo, *to be published*.
[59] F. Carstoiu, L. Trache, C. Gagliardi, R. Tribble, A. Mukhamedzhanov, Phys. Rev. C 63 (2001) 054310.
[60] Z.-H. Liu, J.-D. Bao, Chin. Phys. Lett. 21 (2004) 457.
[61] F. Carstoiu, L. Trache, C. Gagliardi, A. Mukhamedzhanov, R. Tribble, Roman. Rep. Phys. 59 (2007) 357.
[62] I. Angeli, K. Marinova, At. Data Nucl. Data Tables 99 (2013) 69.
[63] A. Estradé, R. Kanungo, W. Horiuchi, F. Ameil, J. Atkinson, Y. Ayyad, D. Cortina-Gil, I. Dillmann, A. Evdokimov, F. Farinon, H. Geissel, G. Guastalla, R. Janik, M. Kimura, R. Knöbel, J. Kurcewicz, Y. Litvinov, M. Marta, M. Mostazo, I. Mukha, C. Nociforo, H. Ong, S. Pietri, A. Prochazka, C. Scheidenberger, B. Sitar, P. Strmen, Y. Suzuki, M. Takechi, J. Tanaka, I. Tanihata, S. Terashima, J. Vargas, H. Weick, J. Winfield, Phys. Rev. Lett. 113 (2014) 132501.
[64] K. Sawahata, A. Ozawa, Y. Saito, Y. Abe, Y. Ichikawa, N. Inaba, Y. Ishibashi, A. Kitagawa, S. Matsunaga, T. Moriguchi, D. Nagae, S. Okada, S. Sato, S. Suzuki, T. Suzuki, Y. Takeuchi, T. Yamaguchi, J. Zenihiro, Nucl. Phys. A 961 (2017) 142.
[65] E. Ryberg, C. Forssén, H.-W. Hammer, L. Platter, Eur. Phys. J. A 50 (2014) 170.

Appendix

This Appendix contains in tabular form the cross sections $\mathrm{d}\sigma/\mathrm{d}t$ as a function of the four-momentum transfer squared for p^8B and p^7Be elastic scattering measured in the present experiment. Only statistical errors are indicated.

p^8B, E_p=702 MeV		p^8B, E_p=702 MeV	
$-t$, $(\mathrm{GeV}/c)^2$	$\mathrm{d}\sigma/\mathrm{d}t$, $\mathrm{mb}/(\mathrm{GeV}/c)^2$	$-t$, $(\mathrm{GeV}/c)^2$	$\mathrm{d}\sigma/\mathrm{d}t$, $\mathrm{mb}/(\mathrm{GeV}/c)^2$
0.00117	9060 ± 207	0.01548	1294 ± 47
0.00164	5876 ± 125	0.01684	1152 ± 43
0.00211	4776 ± 133	0.01826	1002 ± 40
0.00258	4043 ± 123	0.01973	946.9 ± 38.2
0.00305	3555 ± 124	0.02127	865.5 ± 36.0
0.00352	3343 ± 119	0.02285	791.9 ± 34.0
0.00399	3077 ± 123	0.02450	654.2 ± 30.5
0.00446	3031 ± 113	0.02620	620.9 ± 29.3
0.00493	2765 ± 113	0.02796	551.2 ± 27.3
0.00540	2586 ± 114	0.02978	492.6 ± 25.5
0.00586	2536 ± 104	0.03165	438.9 ± 23.8
0.00633	2348 ± 99	0.03359	403.7 ± 22.6
0.00680	2563 ± 104	0.03558	321.7 ± 20.0
0.00727	2247 ± 99	0.03762	314.1 ± 19.6
0.00774	2138 ± 97	0.03973	273.4 ± 18.1
0.00852	2149 ± 68	0.04189	211.3 ± 15.7
0.00954	1891 ± 62	0.04411	207.3 ± 15.5
0.01061	1853 ± 60	0.04755	160.0 ± 9.5
0.01174	1622 ± 55	0.05233	111.8 ± 7.8
0.01293	1572 ± 53	0.05735	89.7 ± 6.9
0.01418	1296 ± 48		

p^7Be, E_p = 701 MeV		p^7Be, E_p = 701 MeV	
$-t$, $(\mathrm{GeV}/c)^2$	$\mathrm{d}\sigma/\mathrm{d}t$, $\mathrm{mb}/(\mathrm{GeV}/c)^2$	$-t$, $(\mathrm{GeV}/c)^2$	$\mathrm{d}\sigma/\mathrm{d}t$, $\mathrm{mb}/(\mathrm{GeV}/c)^2$
0.00117	6401 ± 171	0.01739	921.6 ± 41.5
0.00164	4317 ± 138	0.01864	931.5 ± 43.0
0.00211	3749 ± 127	0.01993	773.4 ± 39.6
0.00258	3093 ± 115	0.02127	775.1 ± 39.2
0.00305	2795 ± 109	0.02265	664.4 ± 36.0
0.00352	2519 ± 103	0.02407	666.2 ± 35.0
0.00399	2519 ± 102	0.02553	592.5 ± 33.4
0.00446	2338 ± 98	0.02704	567.2 ± 32.4
0.00493	2191 ± 95	0.02860	522.8 ± 31.4
0.00540	1962 ± 90	0.03019	451.8 ± 28.6
0.00586	2011 ± 92	0.03183	416.0 ± 27.3
0.00633	2061 ± 92	0.03351	372.5 ± 23.6
0.00680	1889 ± 88	0.03612	298.3 ± 14.7
0.00728	1873 ± 76	0.03975	248.8 ± 14.0
0.00810	1692 ± 69	0.04355	180.5 ± 11.1
0.00896	1605 ± 68	0.04752	161.8 ± 11.6
0.00986	1546 ± 64	0.05168	120.0 ± 9.5
0.01081	1510 ± 62	0.05600	96.7 ± 8.8
0.01180	1335 ± 59	0.06051	78.3 ± 7.7
0.01283	1350 ± 58	0.06519	51.1 ± 6.3
0.01391	1092 ± 47	0.07005	32.3 ± 5.1
0.01503	1127 ± 52	0.07508	31.7 ± 4.4
0.01619	1020 ± 47	0.08029	21.8 ± 3.6
0.01919	1025 ± 42		